2016

# Development of a Pressure Swing Adsorption (PSA) Cycle for CO2 Capture From Flue Gas Using a 4-Bed PSA Apparatus

Joshua White
*University of South Carolina*

# Development of a Pressure Swing Adsorption (PSA) Cycle for $CO_2$ Capture From Flue Gas Using a 4-Bed PSA Apparatus

by

Joshua White

Bachelor of Science
United States Military Academy, 2006

---

Submitted in Partial Fulfillment of the Requirements

For the Degree of Master of Science in

Chemical Engineering

College of Engineering and Computing

University of South Carolina

2016

Accepted by:

John Weidner, Director of Thesis

James Ritter, Reader

Armin Ebner, Reader

Ralph White, Reader

Lacy Ford, Senior Vice Provost and Dean of Graduate Studies

# DEDICATION

For my parents. For Benjamin. Beat Navy.

# ACKNOWLEDGEMENTS

First I would like to acknowledge the help and guidance of Dr. Ebner and Dr. Ritter. Second I would like to acknowledge the hard work put in by Atikur Rahman, his work made this thesis possible. Thank you to Chuck for helping me build and program the PSA system, without his expertise there would be no experiment. Lastly I would like to thank all my fellow students who helped me get through this program, I couldn't have done it without you.

# ABSTRACT

Pressure swing adsorption is an effective way to capture $CO_2$ from flue gases in energy plants. Pressure swing adsorption utilizes an adsorbent's selectivity to a specific compound to remove it from a feed stream. Zeolite 13X was used for this research to obtain a high purity and recovery of $CO_2$ at a higher feed flow than previous research. The first part of the work was to use in house FORTRAN based Dynamic Adsorption Process Simulator (DAPS) that uses the finite difference method and the time adaptive Differential-Algebraic Equation (DAE) solver called DASPK to narrow down appropriate experiment criteria for the custom built 4-bed Pressure Swing Adsorption (PSA) system.

The second part of the research focused on experimentally confirming the mathematical predictions. Adsorption equilibrium isotherms for $CO_2$ and $N_2$, on zeolite 13X were measured by using a volumetric system from micromeritics ASAP2010. The feed gas considered as a simulated dry flue gas consisting of 15.9% $CO_2$ and balance $N_2$ that was fed at 121 kPa and at 25 °C. Operation pressure range provided by this system is from 0 to 127 KPa. A unique combination of cycle steps consisting of three beds were able to produce high purities (>90%) and high recoveries (>90%) of $CO_2$ in the heavy product. The throughput achieved experimentally was 404 $L_{STP}$/hr/kg. The PSA cycle consist of seven different cycle steps; feed (F), heavy reflux (HR), pressure equalization (E), counter-current blowdown, light reflux purge (LR), and light product pressurization (LPP). The model successfully predicts the pressure and temperature profiles and performance of each experiment.

# TABLE OF CONTENTS

# LIST OF TABLES

# LIST OF FIGURES

# CHAPTER 1

# INTRODUCTION

Coal and natural gas fired power plants account for over 60% of the nation's energy production (Department of Energy). From this energy generation, the US produced 3.1 million metric tons of $CO_2$ (Department of Energy). This release of $CO_2$ is known to be a major contributor to global warming. The world at large is working on ways to decrease their dependence on coal for energy, however it is estimated that by 2030, 28% of the world's energy will still come from coal. These coal-fired power plants presents large point sources for $CO_2$ emissions and considerable effort has been underway worldwide to curb $CO_2$ emissions from these large point sources. An average flu gas stream is around 10-15 mol % of CO2. Given this concentration, an average coal fired power plant delivers 800 kg of CO2 per MWh (Webley). The goal is to capture $CO_2$ from the flue gas of power plants and concentrate it to around 90 to 95% and sequester it underground (DOE/NETL).

There are several technologies available to separate $CO_2$ such as absorption, cryogenic distillation, adsorption, and membrane separation. However, to date none of the technologies is economically feasible; so, significant research effort is being undergoing to come up with an economically feasible process to capture $CO_2$. Among the available technologies, physical absorption using amines is the most widely accepted technology. The basic process of amine scrubbing, which was patented in 1930, is the run the flue gas through a scrubber filled with an amine solution. Most commonly 20-30% methylethylamine (MEA) is utilized in full scale processes. The $CO_2$ is absorbed by the

amine solution which is the stripped with water vapor in order to regenerate the MEA. The saturated water vapor can then be condensed leaving pure $CO_2$ which can then be pressurized and sequestered (Rochelle). However, the operating cost is significantly higher in the amine absorption to regenerate the solvent. The amine absorption process takes out a portion of the process steam of the power plant reducing the overall capacity of the power plant. The energy penalty of the cryogenic distillation is prohibitively high. The average energy cost for $CO_2$ capture is between 64.5 and 89.3 kJ/mol of $CO_2$ removed. This process is predicted to become more efficient with a goal of 34.9 kJ/mol of $CO_2$ removed (Rochelle). The membrane process suffers some serious drawbacks such as low flux, degradation, fouling, capital cost and stability at the extreme process conditions.

An article published by the International Energy Agency (IEA) in 1994, focused the use of adsorption technologies for $CO_2$ capture from flue gases on the basis of 500 MW power plant (International Energy Agency). Both pressure swing adsorption (PSA) and temperature swing adsorption (TSA) were evaluated used a commercial adsorbent 13X zeolite. At that time the study clouded that both PSA and TSA were too energy intensive and not feasible for $CO_2$ capture from power plants. In 2003 another report by IEA reiterated the same results (Internal Energy Agency). However Webley and co-workers questioned findings of both report in one of their work (Chaffee, Knowles and Liang). This work reevaluated the PSA process by calculating the energy consumption by a PSA process for $CO_2$ capture to be \$67/tonne $CO_2$ captured compared to \$97/tonne $CO_2$ captured as reported by IEA. This new energy consumption value of PSA compare much more favorably to the energy consumption by the amine absorption process at \$60/tonne $CO_2$. The cost of PSA can be brought down significantly by proper design of the PSA cycle.

Many industries have been developing pressure swing adsorption (PSA) for years. Japanese power industries started developing cyclic PSA/VSA for $CO_2$ removal in early nineties (Hirose, Omori and Oba; Ishipashi, Ota and Akutsu; Ito, Otake and Itoi; Sasaki, Matsumoto and Fujitsuka; Yokoyama). Since early ninety, a number of different PSA/VSA cycle have been developed and reported in the literature. A summary of these studies is tabulated in Table 1.1. The definition of different variables used in the table are, $y_f$ is the % of $CO_2$ in the feed, $p_{CO2}$ and $r_{CO2}$ are the purity and recovery of $CO_2$ in the heavy product stream. However, most of the studies listed in Table 1 are bench-scale studies with extremely small feed throughput.

Ritter research group has studied a number of different cycles of PSA for $CO_2$ capture at high temperature using K-promoted hydrotalcite as the adsorbent (Reynolds, Ebner and Ritter 531-536; Reynolds, Ebner and Ritter 334-342; Reynolds, Ebner and Ritter 4278-4294). Their main emphasis was to obtain heavy product at a high purity by introducing a heavy reflux step. In their work, they compared seven different 4-bed 4-step, 4-bed 5-step and 5-bed 5-step configurations with and without heavy reflux step. In another study, they compared nine different PSA configurations to maximize the $CO_2$ purities and recoveries, however all were at a very small feed throughput (Reynolds, Mehotra and Ebner). Kikkinides et al was able to improve the purity and recovery of $CO_2$ in a 4-bed 4-step process by allowing significant breakthrough of $CO_2$ from the light end of the column undergoing heavy reflux after that recycling the effluent from this light end back to the column with the feed (Kikkinides, Yang and Cho). Chue et al. studied a 3-bed 9-step VSA process using activated carbon and zeolite 13X (Chue, Kim and Yoo). They concluded that zeolite 13X performs better that the activated carbon despite having a high heat of

Table 1.1 PSA cycles suggested in the literature for post-combustion CO2 separation

| PSA Cycle configuration | Operating step sequence[a] | Ads[b] | $y_f$ [%] | $p_{CO_2}$ [%] | $r_{CO_2}$ [%] | $P_l$ [kPa] | Feed throughput [$L_{STP}.hr^{-1}\ kg^{-1}$] | Energy [kJ/mol $CO_2$] | Ref. |
|---|---|---|---|---|---|---|---|---|---|
| 2-stage 5-step and 6-step respectively | (FP,F,HR,CnD,LR) + (FP,F,PE,CnD,LR,PE) | 5A | 15 | 96.0 | 91.0 | 10 | 54.45 | 28.41 | (Liu, Grande and Li) |
| 1-bed 4-step | FP,F,CnD,LR | AC | 15 | 63.0 | 96.0 | 10 | - | - | (Lopez, Grande and Rodrigues) |
| 2-bed 8-step | (FP+HPP),F,HR,PE,CnD,CnD,LR,PE | 13X | 15 | 90.0 | 85.0 | 5 | - | 110.9[e] | (Agarwal, Biegler and Zitney) |
| 2-bed 6-step | (F+REC),(F,PF),HR,CnD,CnD,LR | 13X | 15 | 95.0 | 80.0 | 5 | - | 7.60[e] | (Agarwal, Biegler and Zitney) |
| 1-bed 4-step | F,CoD,CnD,LPP | 13X | 15 | 90.0 | 90.0 | 3 | 420.66* | 20.75 | (Haghpanah, Nilam and Rajendran) |
| 1-bed 4-step | FP,F,CnD,LR | 13X | 15 | 36.8 | 90.0 | 10 | - | - | (Dantas, Luna and Silva)[c,d] |
| 2-bed 8-step | I-FP-F-Eq-CnD-LR-I-Eq (bottom Eq) | AC | 12 | 50.7 | 89.4 | 10 | - | - | (Marx, Joss and Hefti) |
| 2-bed 4-step | FP-F-CoD-CnD | 13X | 15 | 95.9 | 86.4 | 10 | 258.93* | 74.8 | (Krishnamurthy, Rao and Guntuka)[c,d] |
| 1-bed 3-Step | F-CnD-LPP | 13X | 15 | 90 | 90 | 1 | - | - | (Ling, Ntiamoah and Xiao) |
| 2-bed 6-step | F-Eq1-CnD-Eq2-LPP | 13X | 15 | 95 | 90 | 10 | - | - | (Ling, Ntiamoah and Xiao) |

[a]Cycle-step legend: CnD-counter-current depressurization; CoD-co-current depressurization; FP-feed pressurization; F-feed or adsorption; HPP-heavy product pressurization; HR-heavy reflux; LEE-light end equalization; LPP-light product pressurization; LR-light reflux; N-null or idle; R-recycle. [b]Adsorbent legend: HTlc-K-promoted Hydrotalcite; NaX, 13X-molecular sieve zeolites; AC-activated carbon. [c]Studies with experimental results. [d]Multicomponent study.
*assumed a bulk density of 710 kg/$m^3$

adsorption. Zeolite 13X outperforms activated carbon because of its higher working capacity, lower purge requirement and higher equilibrium selectivity. Kikkinides et al was able to improve the purity and recovery of $CO_2$ in a 4-bed 4-step process by allowing significant breakthrough of $CO_2$ from the light end of the column undergoing heavy reflux after that recycling the effluent from this light end back to the column with the feed (Kikkinides, Yang and Cho). Chue et al. studied a 3-bed 9-step VSA process using activated carbon and zeolite 13X (Chue, Kim and Yoo). They concluded that zeolite 13X performs better that the activated carbon despite having a high heat of adsorption. Zeolite 13X outperforms activated carbon because of its higher working capacity, lower purge requirement and higher equilibrium selectivity. PSA cycle employing both heavy and light reflux steps were investigated by Takamura et al (Takmura, Narita and Aoki) and Park et al. (Park, Beum and Kim). Park et al. compared three different configurations of VSA process while Takamura et al. investigated a 4-bed 8-step VSA process. Although the pure $CO_2$ rinse step improved the $CO_2$ purity and recovery, it did not decrease the power consumptions. The power requirements for the 2-bed 6-step and 3-bed 5-step cycle were 106.91 kWh/tonne $CO_2$ and 147.64 kWh/tonne $CO_2$ respectively. However, the feed throughput was quite low (0.331 kgmol/hr) in those studies. Gomes et al. (Gomes and Yee), studied the 2-bed 4-step Skarstrom cycle. He did not employ vacuum to recover $CO_2$. Their study also shows that the pure heavy component cannot be achieved by employing only the light reflux step.

Chou et al. (Chou and Chen) studied two different PSA configurations consisting of 2-bed and 3-bed respectively. The 2-bed process did not have any light or heavy reflux

step while the 3-bed process used both light and heavy reflux steps. Flow reversal was implemented in between the pressurization and depressurization steps in the 2-bed process. The maximum $CO_2$ purity achieved was 63% using a 3-bed 6-step cycle. In a study, Ko et al. (Ko, Siriwardane and Biegler) were able to achieve a $CO_2$ purity of 90% and $CO_2$ recovery of 94% by an optimized 1-bed 4-step fractionated VPSA process. Grande et al. (Grande, Cavenati and Rodrigues), studied 3-bed 5-step process which include a pure $CO_2$ rinse step after the adsorption step. They were able to achieve a purity of 83% and a recovery of 66% at a very high feed throughput of 48.57 kmol/hr. Chaffee et al. (Chaffee, Knowles and Liang) studied a 3-bed 6-step VSA process at a feed throughput of 0.193 kgmol/hr and were able to achieve a lower power consumption of 192 kWh/ton $CO_2$. On the other hand Zhang et al. (Zhang, Webley and Xiao) achieved a power consumption of 240 kWh/ton $CO_2$ at the same feed throughput of 0.193 kWh/ton $CO_2$ with a 3-bed 9-step VSA process. Xiao et al. (Xiao, Webley and Li) achieved a $CO_2$ recovery of 75% with a similar 3-bed 9-step cycle. Zhang and Webley (Zhang and Webley, Cycle Development and Design for CO2 Capture from Flue Gas by Vacuum Swing Adsorption) investigated a number of different VSA configurations and concluded that, by incorporating heavy reflux and equalization steps $CO_2$ purity can be increased.

The main objective of the current study is to develop a PSA process to capture CO2 from the flue gas containing 15% $CO_2$ and balance $N_2$ using 13X zeolite. It is very important to have a reliable process simulator to design any process. The in-house FORTRAN based dynamic adsorption process simulator (DAPS) was validated by fitting the experimental results of the PSA experiment conducted in a single bed apparatus using PSA experiment performed in a single bed PSA apparatus.

# CHAPTER 2

# MATHEMATICAL MODEL

Simulations of the PSA cycles were carried out using an in house dynamic adsorption process simulator (DAPS) developed in FORTRAN that uses the finite difference method and the time adaptive DAE solver called DASPK. The following assumptions are imposed: the ideal gas law, plug flow, no heat transfer limitations between gas and solid (i.e., pellet) phases, no thermal capacitive role of the wall, no axial mass and thermal dispersion, the gas phase concentration in both bulk and pellet porosity is identical, and the mass transfer between solid and gas is defined by 1 parameter macropore limited non-isothermal model. Temperature of the wall set at a constant value equal to the temperature of the bed and heat loss to the exterior defined by heat transfer at the inner side of the wall.

For an N-component PSA process, the overall (O.M.B.) and component mass balances (C.M.B.) over a differential volume element respectively yields:

$$\left(\varepsilon_b + (1-\varepsilon_b)\varepsilon_P\right)C_T\left(\frac{1}{P}\frac{\partial P}{\partial t} - \frac{1}{T}\frac{\partial T}{\partial t}\right) + \varepsilon_b \frac{\partial v C_T}{\partial z} + \sum_{j=1}^{n} S_j = 0 \qquad (1)$$

$$\left(\varepsilon_b + (1-\varepsilon_b)\varepsilon_P\right)C_T \frac{\partial y_i}{\partial t} + \varepsilon_b C_T v \frac{\partial y_i}{\partial z} - y_i \sum_{j=1}^{n} S_j + S_i = 0 \quad i = 1 \text{ to } N\text{-}1 \qquad (2a)$$

$$y_i + \sum_{j=1, j\neq i}^{n} y_j = 0 \quad i = N \qquad (2b)$$

with

$$C_T = \frac{P}{RT};\ S_i = (1-\varepsilon_b)\rho_P \frac{\partial q_i}{\partial t}$$

where $\varepsilon_p$ and $\rho_p$ are the pellet porosity and density, respectively, $\varepsilon_b$ is bulk porosity, $v$ is the interstitial velocity, $y_i$ is the molar fraction of species i in the gas phase, $T$ is the temperature of both gas and solid phases, $P$ is the pressure and $q_i$ is loading of species $i$ in the solid phase, R is the universal gas constant.

To determine the mass transfer rate for the particle for each gas one parameter non-isothermal macro pore model was used. The mass transfer of species $i$ between the solid and gas phase is defined given by Eq. (3):

$$\frac{dq_i}{dt} = k_{M,eff}(q_i^*(P,T) - q_i) \tag{3}$$

where $k_{M,eff}$ is the overall effective macropore mass transfer coefficient, $q_i^*$ is the adsorbed equilibrium concentration, i.e., $q_i^* = f(P,T)$ given by the isotherm and $q_i$ is the average adsorbed concentration.

The overall effective macropore mass transfer coefficient is given by Eq. (4):

$$k_{M,eff} = \frac{1}{1+\frac{RT\rho_p}{\varepsilon_p}\frac{\partial q^*}{\partial P}_{T,P_i}} k_M \tag{4}$$

where $\rho_P$ is the particle density, $\varepsilon_P$ is the particle porosity, $\frac{\partial q^*}{\partial P}_{T,\bar{P}}$ is the slope of the isotherm, $k_M$ macorpore mass transfer parameter. The fitting parameter for this model is $k_M$.

The equilibrium loading of component $i$, $q_i^*$ is calculated from the Three Process Langmuir isotherm Eq. (5):

$$q_i^* = \sum_{k=1}^{3} \frac{b_{i,k} P_i q_{i,k,s}}{1 + \sum_{j=1}^{n} \left(b_{j,k} P_j\right)} \tag{5}$$

where

$$b_{i,k} = b_{i,k,o} \exp\left(\frac{B_{i,k}}{T}\right)$$

and

$$q_{i,k,s} = q_{i,k,s}^* + q_{i,k,st} * T \quad [k = 1 \text{ to } 3]$$

where $q_i^*$ is the total loading of component i in mol/kg, n is the number of components, $q_{i,k,s}$ is the saturation loadings of component i in mol/kg on sites k, $P_i$ is the partial pressure of component I, $T$ is the temperature in K.

The energy balance (E.B.) is expressed as Eq. (6):

$$(\varepsilon_b + (1-\varepsilon_b)\varepsilon_P)\left(Cp_g C_T \frac{\partial T}{\partial t} - \frac{\partial P}{\partial t}\right) + \left((1-\varepsilon_b)\rho_P Cp_p\right)\frac{\partial T}{\partial t} + \varepsilon_b Cp_g C_T v \frac{\partial T}{\partial z} +$$
$$(1-\varepsilon_b)\rho_P \sum_{j=1}^{n}\left(Cp_{a,j} q_j \frac{\partial T}{\partial t} + \Delta H_i \frac{\partial q_i}{\partial t}\right) + \frac{2}{r_{b,i}} h_w (T - T_w) = 0 \quad (6)$$

with

$$Cp_g = \sum_{i=1}^{n}\left(y_j Cp_{g,i}\right)$$

where $Cp_{g,i}$ and $Cp_{a,j}$ are the molar heat capacities of species $i$ in the gas and adsorbed phase, respectively (typically assumed identical), $Cp_p$ is the heat capacity of the pellet, $\Delta H_i$ is the heat of adsorption of species $i$, $h_w$ is the heat transfer coefficient at the inner side of the wall of the bed and $r_i$ is the internal radius of the bed and $T_w$ is the wall temperature.

The pressure drop along the bed is evaluated via Ergun's equation, i.e. the momentum balance (E.B.) Eq. (7):

$$\frac{\partial P}{\partial z} + 1.5\times 10^{-1}\mu_g \left(\frac{1-\varepsilon_b}{2 r_p \varepsilon_b}\right)^2 v + 1.75\times 10^{-3} C_T M_g \frac{1-\varepsilon_b}{2 r_p \varepsilon_b} v|v| = 0 \quad (7)$$

where $\mu_g$ and $M_g$ are the viscosity and the average molecular weight of the gas phase and $r_p$ is the effective radius of the pellet.

At given boundaries the flow rate (F) whether it's goes in or out of the bed is defined according to the valve equation (V.E.), which is defined according to Eq (8):

$$F = C_v v_{sign} \frac{1}{\sqrt{S_g T_-}} \min\left(49.08\left|P_-^2 - P_+^2\right|^{0.5}, 41.63 P_-\right) \quad (8)$$

where $c_v$ is the valve coefficient, $S_g$ is the molecular weight of the gas relative to that of air, $P_-$ and $P_+$ is the pressure upstream and downstream the valve, $T_-$ is the temperature upstream the valve.

The equations described above constitute a complete mathematical model for multi-component pressure swing adsorption process once the initial and boundary conditions for particular steps are specified. For a system containing N components, there are a total of 2N+3 variables and equations that have to be solved at each node.

The initial and boundary conditions depends on the PSA process cycle configuration used. The initial and boundary conditions for different steps are given in Table 2.1.

Table 2.1 Initial and boundary conditions for different steps of the PSA process

| Step | Time and Bed Location | Initial, Boundary conditions and balances |
|---|---|---|
| | | |
| | | |
| **Initial Condition** | | $Y^{step=i+1}(t=0,z) = Y(t = t^{i}_{step}, z)$<br>Where, Y = yi, qi, v, T, P, and i = 1,2……..n |
| | | **Boundary Conditions** |
| **Feed (F)** | z/L = 0 | $y = y_{i,F}$, $F = F_F$, OSIMPM, $T = T_F$, M.B., $P=P_F$, $v = v_F$ (at all t) |
| | z/L = 1 | C.M.B., O.M.B., OSIMPM, E.B. ($T_o = T_F$), V.E. ($P_o=P_H$) (at all t) |
| | | |
| **Heavy Reflux (HR)** | z/L = 0 | $y = y_{i,HR}$, $F = F_{HR}$, OSIMPM, $T = T_{HR}$, M.B., $P=P_{HR}$, $v = v_{HR}$ (at all t) |
| | z/L = 1 | C.M.B., O.M.B., OSIMPM, E.B. ($T_o = T_F$), V.E. ($P_o=P_H$) (at all t) |
| | | |
| **Equalization (E)** | z/L = 0 | C.M.B., v = 0, OSIMPM, E.B. ($T_o = T_F$) (at all t) |
| | z/L = 1 | C.M.B., O.M.B., OSIMPM, E.B. ($T_o = T_F$), V.E. ($P_o=P_H$) (at all t) |
| | | |
| **Counter-current depressurization (CnD)** | z/L = 0 | C.M.B., O.M.B., OSIMPM, E.B. ($T_o = T_F$), V.E. (at all t) |
| | z/L = 1 | C.M.B., v = 0, OSIMPM, E.B. ($T_o = T_F$) (at all t) |
| | | |
| **Light reflux (LR)** | z/L = 0 | C.M.B., O.M.B., OSIMPM, E.B. ($T_o = T_F$), V.E. (at all t) |
| | z/L = 1 | $y = y_{i,LR}$, $F = -F_{LR}$, OSIMPM, $T = T_F$, M.B. (at all t) |
| | | |
| **Equalization (E*)** | z/L = 0 | C.M.B., O.M.B., OSIMPM, E.B. ($T_o = T_F$), v = 0 (at all t) |
| | z/L = 1 | $y = y_{i,E1D,z/L=1}$, $F = -F_{E1D,z/L=1}$, OSIMPM, $T = T_F$, M.B. (at all t) |
| | | |
| **Light Product pressurization (LPP)** | z/L = 0 | C.M.B., v = 0, OSIMPM, E.B. ($T_o = T_F$) (at all t) |
| | z/L = 1 | $y = y_{i,LPP}$, $F = -F_{LPP}$, OSIMPM, $T = T_F$, M.B. (at all t) |

F ($= \varepsilon_b A_b v(P/P^*)(T^*/T)$): Flow in SLPM; C.M.B: Component mass balance; O.M.B: Overall mass balance; O.S.I.M.P.M. One Step Isothermal Macropore Model; E.B.: Energy balance; M.B.: Momentum balance; V. E.: Valve equation

# CHAPTER 3

# EXPERIMENTAL SECTION

## 3.1 ADSORPTION ISOTHERM MEASUREMENT

Pure component adsorption equilibrium isotherms for $CO_2$ and $N_2$, on zeolite 13X were measured by using a volumetric system from micromeritics ASAP2010. Since ASAP-2010 is designed for surface area and porosimetry measurements and measures the nitrogen isotherm at 77 K it had to be modified to be able to measure different pure gas isotherms at various temperatures. Operation pressure range provided by this system is from 0 to 127 KPa. The molecular drag pump can create vacuums down to $1.3 * 10^{-6}$ KPa in the system. The volumetric method involves measuring the pressure change in a known volume of sample gas exposed to an adsorbent sample. As the gas is adsorbed and allowed to come to equilibrium with the adsorbent, the measured decrease of pressure in the closed system indicates the amount of gas adsorbed under the given isothermal conditions.

Data was collected for the equilibrium pressure range of 0.001 to 110 KPa at 25, 50 and 75 degree Celsius. Obtaining each complete isotherm consists of 60 to 120 equilibrium point measurements and takes roughly about 12 hours. For each point when the rate of change for pressure is less than 0.01% criterion for equilibrium is satisfied and the system moves to the next point.

Prior to each isotherm measurement, the zeolite 13X was regenerated at 350 °C for 16 hours under a vacuum of less than $1 \times 10^{-4}$ torr. In order to prevent structural damage caused by desorbing water steam. A stepwise increase in temperature with simultaneous

vacuum was applied to all samples. The pure gas adsorption isotherm along with the model fit has been shown in Figure 3.1. The experimentally determined pure gas isotherms except for $CO_2$ have been fitted with the Dual Process Langmuir (DPL) model. The experimental isotherm of $CO_2$ was fitted with three-process Langmuir (TPL) isotherm. The isotherm model parameters have been summarized in Table 3.1.

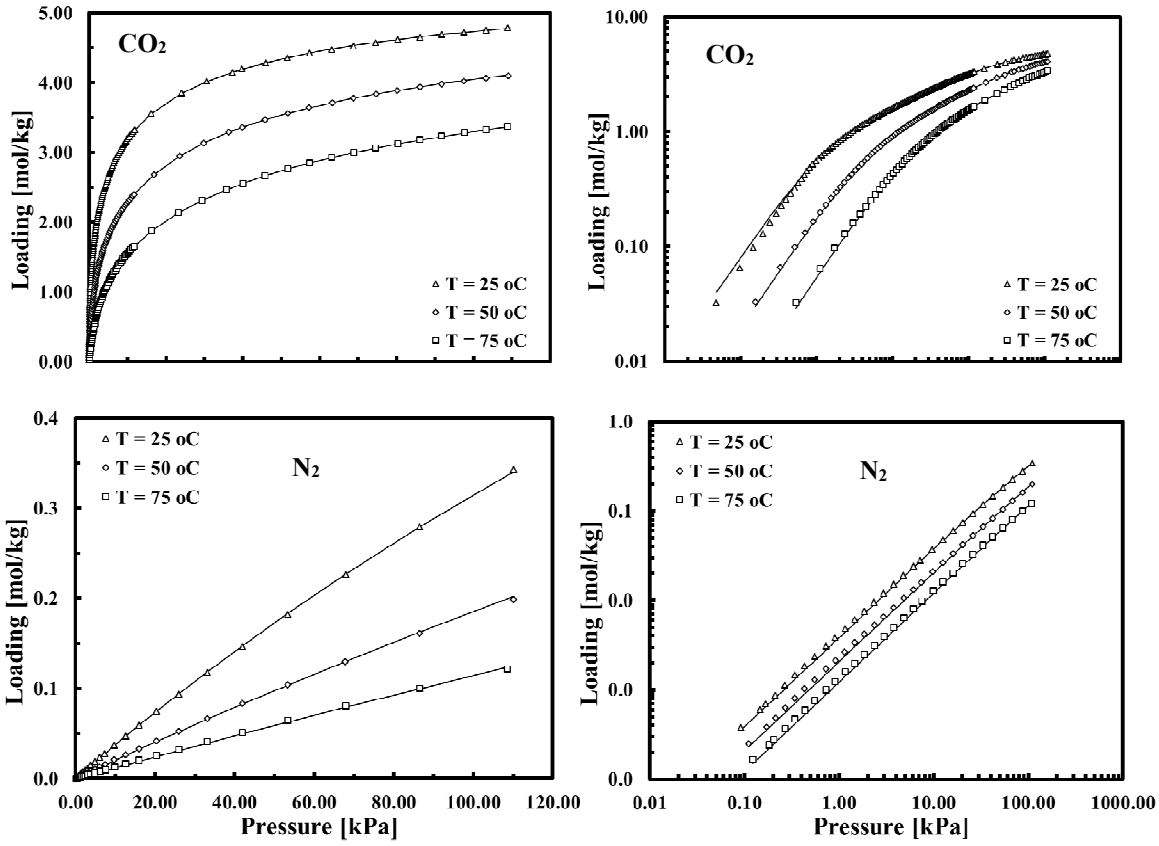


Figure 3.1 Isotherms of Carbon dioxide and Nitrogen at three different temperatures in linear (left) and log-log scale (right). The solid lines represent the model fits and the markers represent the experimental data.

Table 3.1 Three process Langmuir isotherm parameters for $CO_2$ and $N_2$

| Parameter | $CO_2$ | $N_2$ |
|---|---|---|
| **ns1 [mole/kg]** | 1.338 | 0.438 |
| **ns2 [mole/kg]** | 2.238 | 0.733 |
| **ns3 [mole/kg]** | 1.853 | 0.607 |
| **b01 [1/kPa]** | 2.4419E-08 | 7.595E-07 |
| **b02 [1/kPa]** | 4.5204E-08 | 7.595E-07 |
| **b03 [1/kPa]** | 1.3737E-08 | 7.595E-07 |
| **B21 [K]** | 5757.03 | 2370.32 |
| **B22 [K]** | 4606.08 | 2370.32 |
| **B23 [K]** | 4224.86 | 2370.32 |

## 3.2 DESCRIPTION OF 4-BED PSA APPARATUS

A complete and detailed schematic diagram of the 4-bed PSA apparatus is shown in Figure 3.2. This is a lab scale fully functional complete PSA experimental setup. There are identical four adsorbent beds, each was packed with 13X zeolite beads. There are multiple valve manifold on top and bottom of each bed. By opening and closing each valves, a number of flow configuration in and out of each bed can be obtained. For example, for bed-1, at the top of the bed valve-1 was used to withdraw light product during the feed step, valve-2 was opened to equalize with another bed during the pressure equalization step, valve 38 was opened to withdraw the light product produced during the heavy reflux step, valve-3 was opened to feed the light product during the light reflux step,

and valve 45 was used to pressurized the bed from the light end with light product. At bottom of the bed-1, valve 6 was opened to introduce the feed gas to the bed, valve-5 was opened during the counter current blowdown step to withdraw the heavy product, and valve-4 was used to feed the bed during the heavy reflux step. Four flow controllers F21, F22, F23 and F24 are used to blend individual pure gas to form the desired feed concentration. In this case, F22 was used for $N_2$ and F23 was used for $CO_2$, by setting appropriate flow rate of F22 and F23 the simulated flue gas containing 15% $CO_2$ in $N_2$ was produced. Each bed has dedicated line for feed, light product (LP), heavy product (HP), reflux gas isolated by several trains of solenoid valve. For example, Bed 1, 2, 3 and 4 were

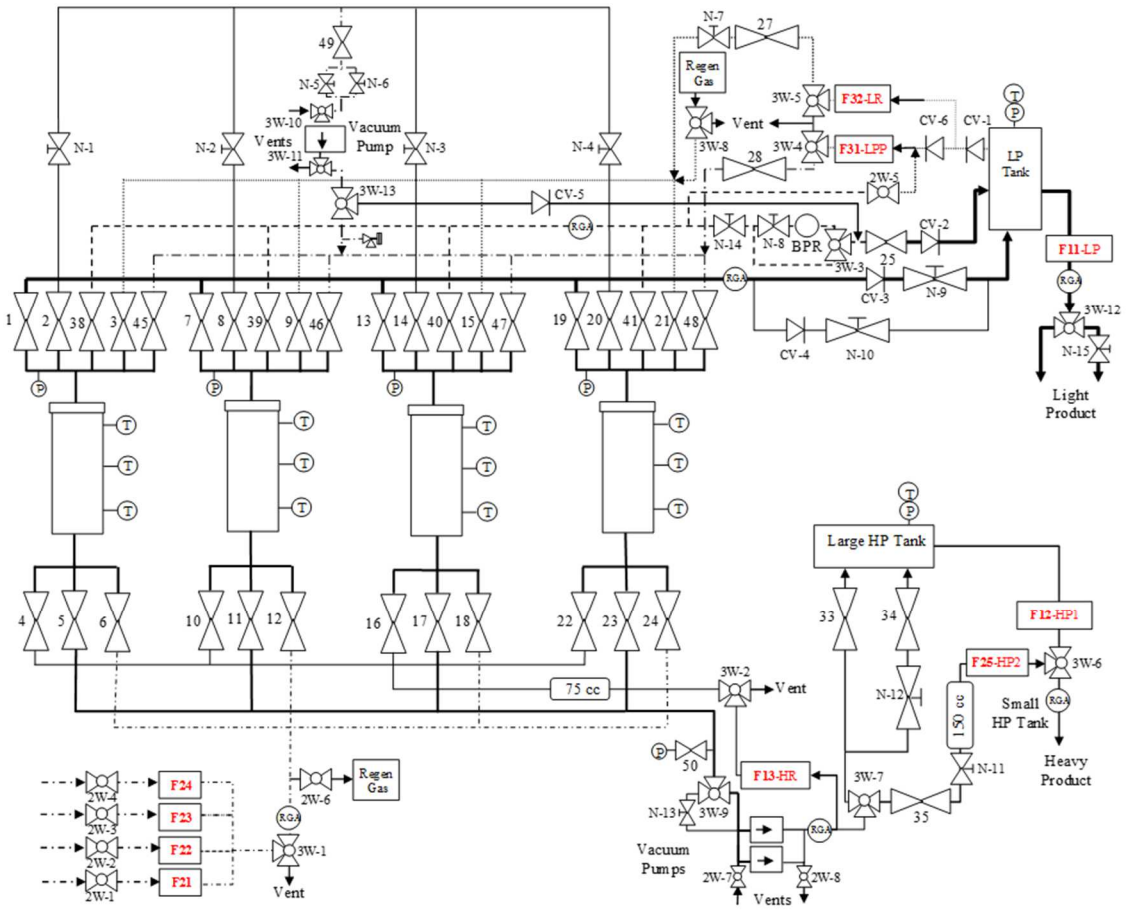


Figure 3.2 A detailed schematic of the 4-bed PSA apparatus

fed by opening valve 6, 12, 18 and 24 respectively. The light product was drawn from each bed by opening valve 1, 7, 13 and 19 and sent to the light product tank (LP Tank). The PSA cycle studied in this study is a 3-bed 7-step process, so only bed 1, 2 and 3 were used and bed-4 was kept isolated by closing all the valves connected to it. Seven exposed tip, K-type thermocouples were placed axially along the column to measure the temperature profiles. Bed 2, 3 and 4 has only three thermocouple across the bed. The temperature profiles provided an estimate of position of the concentration wave fronts within the column. A pressure transducer was placed few inches above each column to measure the column pressure. The solenoid valves were operated using a spreadsheet based LabVIEW software and different process parameters were recorded in the computer using the same software.

## 3.3 PSA EXPERIMENTS

The PSA cycle consist of seven different cycle steps namely feed (F), heavy reflux (HR), pressure equalization (E), counter-current blowdown, light reflux purge (LR), and light product pressurization (LPP). The cycle schedule studied is shown in Table 3.2 and a simple schematic diagram is shown in Figure 3.3. Simulated flue gas containing 15% $CO_2$ in $N_2$ was produced by blending pure $CO_2$ and $N_2$ using flow controller F23 and F22 respectively. Each flowmeter was calibrated using a gilibrator for every gas. Details of each of these cycle steps are given below:

The first step of the PSA cycle is the feed step (F) where simulated flue gas (16% $CO_2$ and 84% $N_2$) enters bed-1 at high pressure $P_H$ through the heavy end or the feed end of the bed by opening valve 6. The heavy gas, $CO_2$ is preferentially adsorbed whereas $N_2$

rich gas leaves the column from the other end via valve 1 and enters the light product tank. The pressure of the bed remains constant during the F step and is equal to the highest operating pressure in the cycle denoted by $P_H$. A small portion of the light product was sent to bed-3 at low pressure $P_L$ from the light product tank by setting the appropriate flow in flow controller F31 via valve 15 during the light reflux step. All of the light reflux gas coming out of bed-3 via valve 17 was sent to bed-2 via valve 10 to perform heavy reflux step. Flow meter F13 was used to record the flow of the heavy reflux gas. After the feed step, bed-1 undergoes heavy reflux step, the gas as enters bed-1 at the high pressure $P_H$ during this step via valve 4 and exit the bed via 1. When bed-1 undergoes heavy reflux step, bed-2 undergoes light reflux step. The light reflux gas enters bed-2 via valve 9. After undergoing the HR step bed-1 then equalizes with bed-2. Valve 2 of bed-1 and valve 8 of bed-2 were opened the pressures of these two bed were allowed to equalize and pressure of both bed becomes $P_E$. After the pressure equalization, step bed-1 was emptied counter currently by exposing it to the vacuum pump to low pressure $P_L$ while keeping the other end closed. The pressure of the bed-2 While bed-1 and bed-2 undergoing pressure equalization step, the pressure of bed-3 was brought back to the feed temperature $P_H$ by light product pressurization step by feeding the light product via valve 47. All three beds in the process undergoes the above mentioned seven steps in a cyclic manner.

Table 3.2 PSA cycle schedule

| FEED | | | HR | E | CnD | LR | E* | LPP |
|---|---|---|---|---|---|---|---|---|
| HR | E | CnD | LR | E* | LPP | FEED | | |
| LR | E* | LPP | FEED | | | HR | E | CnD |
| 120 | 20 | 100 | 120 | 20 | 100 | 120 | 20 | 100 |

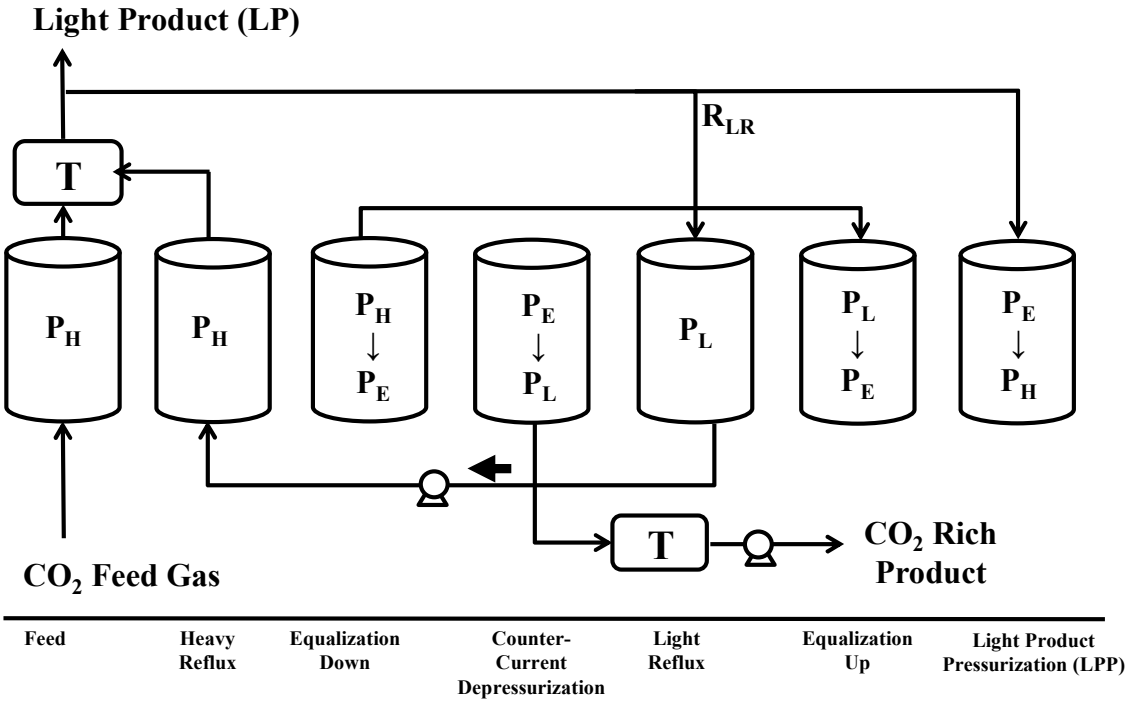


Figure 3.3 Schematic diagram showing various cycle steps in a 3-bed 7-step dual-reflux stripping Pressure Swing Adsorption cycle with one equalization step. All the gas exiting from the light reflux (LR) step is taken out as heavy product (HP).

## 3.4 PSA CYCLE PROCESS PERFORMANCE INDICATORS

The PSA process was designed to produce enriched $CO_2$ as the heavy product and take out $N_2$ in the light product. The periodic state recovery and purity of $CO_2$ in the heavy product and the recovery and purity of the $N_2$ in the light product was used to judge the overall performance of the process, the average mole fraction of $CO_2$ in the heavy product during the CnD step was taken as the purity of $CO_2$ in the heavy product. The average mole fraction was calculated by averaging the mole fraction of the streams coming out of the CnD step. The recovery of this process was defined as the total amount of $CO_2$ produced divided by the total amount of $CO_2$ fed during the feed. The $N_2$ recovery in the light product

is defined as the total moles of $N_2$ produced in the light product divided by the total amount of $N_2$ fed during feed, HR, LR and LPP steps.

A total of twenty runs were carried out to study the effect of different process parameters on the overall process performance. The parameters studies was the light reflux ratio, CnD pressure, feed concentration, bed temperature. The bed properties and run conditions during each run (Runs 1 to 6) are shown in Table 3.3.

The performance indicators of the PSA process are evaluated in terms of purity, recovery and throughput, which are defined below for feed concentration $y_F$ of $CO_2$:

$$\text{Purity}(\%)=\frac{CO_2(\text{mol})\text{obtained as product during A step.100}}{\text{total Product(mol)obtained during A step}} \tag{9}$$

$$\text{Recovery}(\%)=\frac{CO_2(\text{mol})\text{obtained as product during CnD step.100}}{COH_2(\text{mol})\text{ fed during Feed step}} \tag{10}$$

$$\text{Throughput}\left(\frac{\text{L(STP)}}{\text{kg.h}}\right)=\frac{\text{Fresh total Feed(L(STP)) used in Feed step.60}}{\text{Mass of adsorbent(kg)in all beds}} \tag{11}$$

The compressor energy was calculated using the following formula:

$$E_i\left(\frac{\text{kj}}{\text{mol}}\right)=\frac{1}{n_{CO_2}}\int_0^{t_{step}}\left(\frac{\gamma}{\gamma\text{-}1}\right)RT\left[\left(\frac{P_{high}}{P(t)}\right)^{\frac{\gamma\text{-}1}{\gamma}}\text{-}1\right]\frac{1}{\eta}n(t)dt \tag{12}$$

where $t_{step}$ is the duration of the step feeding the compressor, $n_{CO2}$ is the total moles of $CO_2$ removed into the heavy product (HP) per cycle during the CnD step and P(t) and n(t) are the time varying pressure and molar flow, respectively, of the stream being fed into the compressor.

Table 3.3 Bed properties and operating conditions

| Properties | Values |
|---|---|
| **Bed Characteristics** | |
| Length (m) | 0.50165 |
| Internal Radius (m) | 0.0254 |
| Bed porosity | 0.425 |
| Bulk density (kg/m$^3$) | 632.8 |
| External Heat transfer Coefficient (kW/m$^2$/K | 0.0024 |
| **Wall** | |
| Material | SS 316 |
| Thickness (mm) | 4.0 |
| Heat capacity (kJ/kg/K) | 0.468 |
| Density (kg/m$^3$) | 8.24 |
| Wall Temperature, $T_W$ (°C) | 25, 70, 100 |
| **Adsorbent** | |
| Material | Zeolite 13X |
| Average mass per bed (kg) | 0.6396 |
| Pellet density (kg/m$^3$) | 1100.0 |
| Pellet porosity | 0.54 |
| Pellet heat capacity (kJ/kg/K) | 1.1 |
| **Operation** | See table 3.2 |
| Feed flow (SLPM) | 13.0 |
| $CO_2$ concentration (Balance $N_2$, %) | 10.0, 15.9 |
| Feed and external temperature (°C) | 25.0 |
| Light reflux ratio* | 0.02-0.05 |
| High pressure, $P_H$ (kPa) | 121.0 |
| Low pressure, $P_L$ (kPa) | 5.0, 7.0, 10.0 |
| Temperature, (°C) | 25, 70, 100 |
| Cycle time (s) | 720 |
| Feed step (s) | 240 |
| Counter current depressurization (CND) step (s) | 100 |
| Light reflux step (LR) (s) | 120 |
| Light product pressurization (LPP) step (s) | 100 |
| Heavy Reflux (HR) step (s) | 120 |
| Equalization (Eq) step (s) | 20 |
| **Gasses** | |
| $CO_2$ | |
| Isotherm | See Table 3.1 |
| Mass transfer Coefficients, $k_{M1}$ (1/s) | 47.21 |
| Nitrogen | |
| Isotherm | See Table 3.1 |
| Mass transfer Coefficient, $k_{M1}$ (1/s) | 70.34 |

*** Volume fraction of the product flow leaving the feed step used in LR step**

# CHAPTER 4

# RESULTS AND DISCUSSION

## 4.1 PSA EXPERIMENTAL RESULTS

A number of PSA experiments were performed in the 4-bed PSA experimental setup to study the effect of different process parameters on the performance of the PSA process. Total twenty runs were carried out to study the effect of various process parameters on the performance of the PSA process. The parameters studied include feed concentration, reflux or purge to feed ratio ($\gamma$) in the light reflux step, CnD pressure ($P_L$) or the pressure ratio ($\pi$) by keeping the high pressure constant ($P_H$) and bed temperature. Table 3.3 summarizes all the process conditions for the run E-1 through E-20. The base case is run 2 (E-2) which was conducted at 70 °C bed temperature, total cycle time was 720 sec, reflux ratio 3% and CnD pressure 5 kPa. The CnD pressure ($P_L$) was controlled by fine-tuning with a needle valve in the vacuum line. The mass balance of all the runs along with the percentage of error was summarized in Table 4.1. The experimental error in all the runs were no more than 4%, which is reasonably accurate.

Figure 4.1 shows the periodic state temperature profiles of three beds during experiment E-1. Only bed-1 is equipped with seven thermocouples (T-1 to T-7) along the bed. Bed 2 and 3 has only three thermocouple placed along the bed at a relative distance of 24.20% (bottom), 47.26% (middle) and 70.31% (top). Figure 4.1 (a-c) shows the periodic state temperature profile of all three beds for the top, middle and bottom thermocouples. Since all the beds undergoes same cycle steps in a sequential manner, the temperature

Table 4.1 Material balance summary with error

| Exp | $CO_2$ Balance [SL/Cycle] | | | $N_2$ Balance [SL/Cycle] | | | Total Balance [SL/Cycle] | | |
|---|---|---|---|---|---|---|---|---|---|
| | In | Out | %Error | In | Out | %Error | In | Out | %Error |
| E-1 | 24.94 | 24.56 | 1.54 | 130.99 | 129.57 | 1.08 | 155.93 | 154.13 | 1.16 |
| E-2 | 25.05 | 24.70 | 1.43 | 131.03 | 127.55 | 2.65 | 156.08 | 152.25 | 2.45 |
| E-3 | 25.05 | 25.51 | 1.84 | 130.98 | 126.95 | 3.08 | 156.03 | 152.46 | 2.29 |
| E-4 | 24.94 | 25.27 | 1.29 | 131.00 | 128.05 | 2.25 | 155.94 | 153.31 | 1.69 |
| E-5 | 24.94 | 24.03 | 3.67 | 130.99 | 129.53 | 1.11 | 155.93 | 153.56 | 1.52 |
| E-6 | 24.94 | 25.01 | 0.26 | 130.99 | 129.30 | 1.29 | 155.93 | 154.31 | 1.04 |
| E-7 | 22.38 | 22.29 | 0.41 | 131.03 | 127.15 | 2.96 | 153.41 | 149.45 | 2.58 |
| E-8 | 22.38 | 21.98 | 1.80 | 131.02 | 127.94 | 2.35 | 153.41 | 149.93 | 2.27 |
| E-9 | 22.38 | 21.97 | 1.84 | 131.01 | 127.22 | 2.90 | 153.40 | 149.19 | 2.74 |
| E-10 | 22.38 | 21.99 | 1.75 | 131.00 | 127.77 | 2.46 | 153.38 | 149.76 | 2.36 |
| E-11 | 15.72 | 15.39 | 2.09 | 140.89 | 138.19 | 1.92 | 156.61 | 153.58 | 1.94 |
| E-12 | 15.71 | 15.89 | 1.12 | 140.85 | 138.34 | 1.78 | 156.56 | 154.23 | 1.49 |
| E-13 | 24.95 | 25.03 | 0.35 | 131.01 | 128.45 | 1.95 | 155.95 | 153.49 | 1.59 |
| E-14 | 24.94 | 24.76 | 0.75 | 130.99 | 129.25 | 1.33 | 155.93 | 154.01 | 1.24 |
| E-15 | 22.38 | 22.01 | 1.64 | 131.00 | 128.57 | 1.86 | 153.38 | 150.58 | 1.83 |
| E-16 | 22.38 | 22.68 | 1.34 | 130.98 | 128.48 | 1.91 | 153.36 | 151.16 | 1.44 |
| E-17 | 24.94 | 24.52 | 1.68 | 130.99 | 129.09 | 1.45 | 155.94 | 153.61 | 1.49 |
| E-18 | 24.92 | 24.88 | 0.17 | 130.89 | 129.00 | 1.44 | 155.81 | 153.88 | 1.24 |
| E-19 | 22.39 | 23.44 | 4.72 | 131.02 | 126.30 | 3.60 | 153.40 | 149.74 | 2.39 |
| E-20 | 22.38 | 21.40 | 4.37 | 131.01 | 126.11 | 3.73 | 153.39 | 147.52 | 3.83 |



21

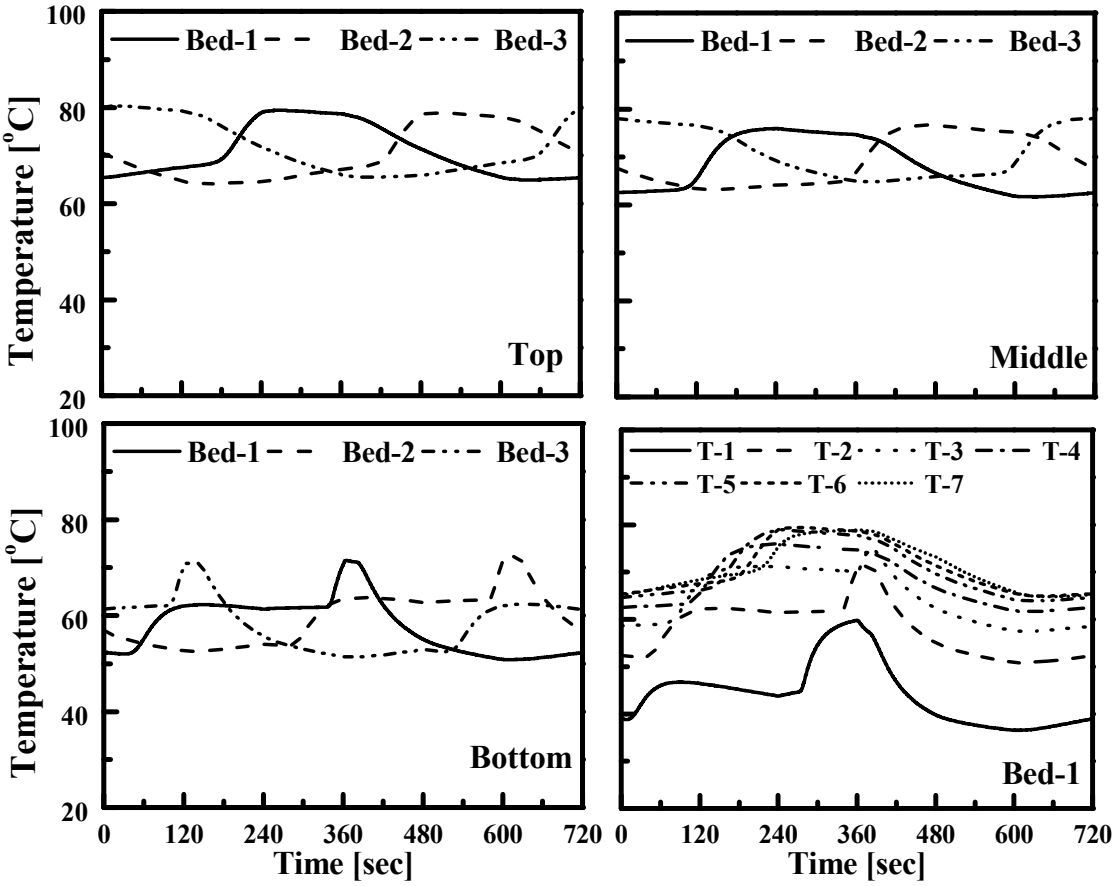


Figure 4.1 Periodic state temperature profiles of bed-1,2 and 3 for the experiment E-1; a) top thermocouple placed at 70.31% of length of each bed, b) middle thermocouple placed at the 47.26% of length of each bed, c) bottom thermocouple placed at the 24.20% of the length of each bed, d) temperature history of bed-1 at 7 different equidistant locations along the bed (1:12.68%, 2:24.20%, 3:35.73%, 4:47.26%, 5:58.78%, 6:70.31%, 7:81.83%).

behavior of all the beds are similar at the periodic state. The periodic state temperature profiles of all seven thermocouples has been plotted in Figure 4.1(d). The temperature profiles shows the progression of the concentration wave through the bed. The first temperature peak corresponds to the temperature rise due to the feed gas. However, the higher temperature peak corresponds to the temperature rise due to higher concentration heavy reflux stream. Figure 4.2(a) shows the periodic state pressure profiles of all three beds for a complete PSA cycle of the run E-1. It is evident from Figure 4.2(a) how the beds

interact with each other during the course of the PSA process and undergoes the same set of cycle steps in a sequential manner. Figure 4.2(b) shows the periodic state pressure profile for bed 1 for the run E-1.

The reflux ratio or the purge to feed ratio ($\gamma$) is the ratio of the flow of the purge gas entering the bed during the LR step to that of the feed gas entering the F step. $\gamma$ is a very important design parameter that has a significant effect on the process performance in terms of recovery and purity of the heavy product (Reynolds, Ebner and Ritter 531-536; Reynolds, Ebner and Ritter 334-342; Reynolds, Ebner and Ritter 4278-4294; Reynolds, Mehotra and Ebner). A large $\gamma$ means a lot of light gas enters the bed during the LR step enhancing desorption of the heavy product from the adsorbent and consequently better adsorbent regeneration. However, a large LR flow dilutes the effluent gas that exits the bed undergoing LR step. For a PSA process where the heavy product is produced from LR step, higher $\gamma$ results in higher $CO_2$ recoveries but lower $CO_2$ purity in the heavy product (Reynolds, Ebner and Ritter 531-536; Reynolds, Ebner and Ritter 334-342; Reynolds, Ebner and Ritter 4278-4294; Reynolds, Mehotra and Ebner). A large $\gamma$ is necessary to better regenerate the bed and reduce the breakthrough of $CO_2$ from the light end of the bed during the F and HR steps. The relative dilute LR effluent can be completely recycled back into the system as feed gas to the bed undergoing the HR step while the heavy product can only be produced only form the CnD step.

Experiments E-1, E-2 and E-3 were performed at three different $\gamma$ by keeping other process parameters the same. Table 4.2 shows that the $CO_2$ concentration in the HR stream decreases as $\gamma$ was increased (E-1 to E-3).

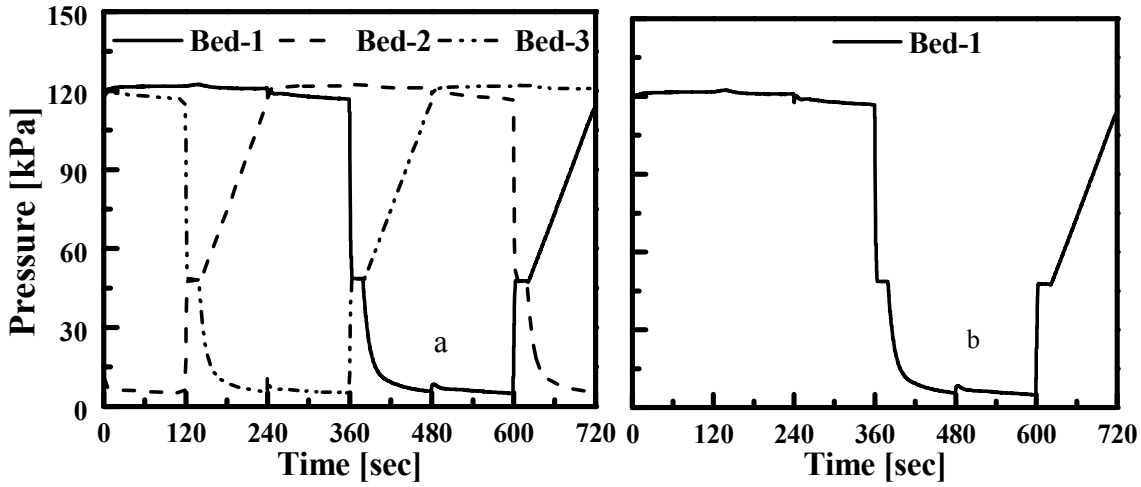


Figure 4.2 Pressure history for all 3 beds during one entire cycle (left) and pressure history for only bed-1 during one entire cycle (right) of experiment E-1.

The purity and recovery increases for increased γ. A high γ implies a higher flow of the purge gas which forces more $CO_2$ to desorb from the adsorbent and exit the bed during the LR step. The bed regenerates better by increasing γ resulting in less $CO_2$ breakthrough during the F step. As a result, the recovery of $CO_2$ in the heavy product increases with increasing γ. However, as the total effluent gas exiting the LR step was recycled back to the HR step, a higher γ pushes the high concentration wave front further down the bed. For a given value of γ chosen for operation, one of two scenarios can happen. The higher concentration wave front can be contained inside of the bed depending on how far it travelled through the bed during the HR step or it might breakthrough through the light of the bed for a higher value of γ resulting in loss of $CO_2$, which causes lower $CO_2$ recovery. The purity also increases as γ was increased. With increasing γ, the high concentration wave front propagates further down the bed during the HR step, which in turn increases the loading of $CO_2$ in the solid phase. All $CO_2$ adsorbed during the HR step subsequently

desorb during the CnD step resulting in a high purity heavy product rich in $CO_2$. However, the higher $\gamma$ also dilutes the effluent coming out of the LR step which enters the LR step. It is clear from the above discussion that the progression of the higher concentration wave front significantly affects the process performances such a $CO_2$ purity, $CO_2$ recovery in the heavy product.

The next important parameter in a PSA process design is the pressure ratio ($\pi$). The pressure ratio ($\pi$) is defined as the ratio of the highest pressure ($P_H$) to the lowest pressure ($P_L$) in the cycle. If the highest pressure $P_H$ is kept constant then a higher $\pi$ implies that the compressors are required to pull a deeper vacuum in the PSA beds during the regeneration steps. The desertion of $CO_2$ from the adsorbent strongly depends upon $\pi$ and thus affects the process performances in terms of $CO_2$ purity and recovery in the heavy product. A higher $\pi$ for a constant $P_H$ means a lower $P_L$, which results in better desorption of $CO_2$ during both CnD and LR steps resulting in higher $CO_2$ bed capacity. Figure 4.3 shows the effect of $\pi$ on $CO_2$ purity and $CO_2$ recovery in the heavy product for a constant throughput of 404 $L_{STP}$/hr/kg. The parameters held constant for each run are bed temperature (70 °C), high pressure ($P_H$ = 120 kPa), purge to feed ration ($\gamma$ = 3%), $CO_2$ feed concentration (16%), feed temperature (25 °C) and total feed flow rate. It is evident that both $CO_2$ purity and recovery decreases by increasing the low pressure PL. More $CO_2$ is desorbed for lower PL (increased $\pi$) and taken as heavy product during the CnD step. More $CO_2$ in the heavy product for lower PL increases the $CO_2$ purity and recovery. Lower PL also helps desorbs more $CO_2$ from the adsorbent thereby increasing the bed capacity resulting in less $CO_2$ breakthrough during F and HR steps.

Table 4.2 Summary of PSA cycle experimental results

| Temp | Exp | Feed $CO_2$ Conc. | $P_L$ | R.R. | $CO_2$ Conc HR | $CO_2$ HP | | $N_2$ LP | |
|---|---|---|---|---|---|---|---|---|---|
| [°C] | | [%] | [kPa] | [%] | [%] | % Pur | % Rec | % Pur | % Rec |
| 70 | E-1 | 16.00 | 5.02 | 2.0 | 85.09 | 96.83 | 91.68 | 98.70 | 98.35 |
| | E-2 | 16.05 | 5.01 | 3.0 | 78.67 | 95.43 | 90.81 | 98.48 | 96.52 |
| | E-3 | 16.05 | 5.12 | 4.0 | 75.07 | 96.54 | 94.06 | 98.48 | 96.28 |
| | E-4 | 16.00 | 7.01 | 3.0 | 80.17 | 94.44 | 82.32 | 96.40 | 96.82 |
| | E-5 | 16.00 | 6.94 | 4.0 | 80.23 | 95.93 | 87.16 | 98.25 | 98.18 |
| | E-6 | 16.00 | 10.28 | 4.0 | 77.12 | 93.68 | 70.39 | 94.50 | 97.80 |
| | E-7 | 14.59 | 5.02 | 2.0 | 85.39 | 95.57 | 88.34 | 98.04 | 96.34 |
| | E-8 | 14.59 | 7.18 | 3.0 | 82.79 | 93.43 | 81.74 | 97.17 | 96.67 |
| | E-9 | 14.59 | 6.97 | 4.0 | 78.23 | 94.01 | 84.22 | 97.59 | 96.20 |
| | E-10 | 14.59 | 9.96 | 4.0 | 79.24 | 91.04 | 71.26 | 95.43 | 96.34 |
| | E-11 | 10.04 | 5.06 | 3.0 | 73.19 | 86.79 | 90.62 | 99.16 | 96.54 |
| | E-12 | 10.04 | 5.06 | 5.0 | 66.76 | 86.46 | 97.01 | 99.53 | 96.52 |
| 100 | E-13 | 16.00 | 5.02 | 3.0 | 81.29 | 97.61 | 93.17 | 98.64 | 97.62 |
| | E-14 | 16.00 | 5.04 | 2.0 | 85.67 | 97.47 | 89.58 | 98.16 | 98.23 |
| | E-15 | 14.59 | 5.03 | 3.0 | 80.51 | 91.23 | 89.76 | 91.23 | 89.76 |
| | E-16 | 14.59 | 5.14 | 2.0 | 90.43 | 94.27 | 89.01 | 97.89 | 97.17 |
| 25 | E-17 | 15.99 | 5.50 | 3.0 | 83.58 | 96.05 | 91.66 | 98.27 | 97.83 |
| | E-18 | 15.99 | 4.97 | 2.0 | 87.73 | 96.81 | 91.68 | 98.44 | 97.98 |
| | E-19 | 14.59 | 4.99 | 3.0 | 90.43 | 94.23 | 92.70 | 97.89 | 95.43 |
| | E-20 | 14.59 | 5.04 | 2.0 | 80.85 | 93.93 | 87.62 | 98.58 | 95.30 |

For a constant feed throughput, total moles entering the system is the same. As a result, if more moles of $CO_2$ is desorbed during the CnD step for a lower PL and removed as a heavy product during the CnD step, which in turn will hamper the progression of the higher concentration wave front through the bed. Despite a higher concentration wave front not penetrating deeper into the bed during the HR step for experiments with lower PL compared to an experiment with higher PL, a large $CO_2$ purity in the heavy product can be obtained provided a deeper vacuum is pulled in the beds.

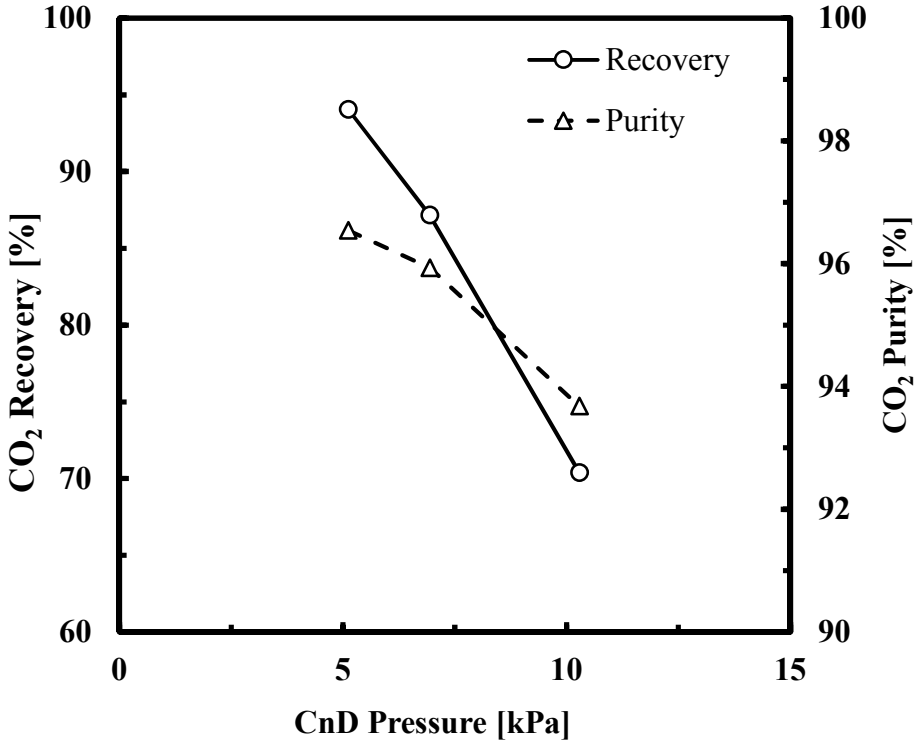


Figure 4.3 Effect of CnD pressure (i.e. pressure ratio, π) on $CO_2$ purity and $CO_2$ recovery in the heavy product.

This proves that the purity of $CO_2$ in the heavy product does not only depend upon the propagation of the higher concentration wave front during the HR step but also on the low pressure during the CnD step.

The effect of temperature on the $CO_2$ recovery and purity is shown in Figure 4.4. Both $CO_2$ recovery and purity decreases initially for 70 °C and then increases in the experiment performed at 100 °C. The temperature plays an important role in determining the working capacity of the adsorbent. A higher temperature also helps desorb the heavy component during the CnD and LR step.

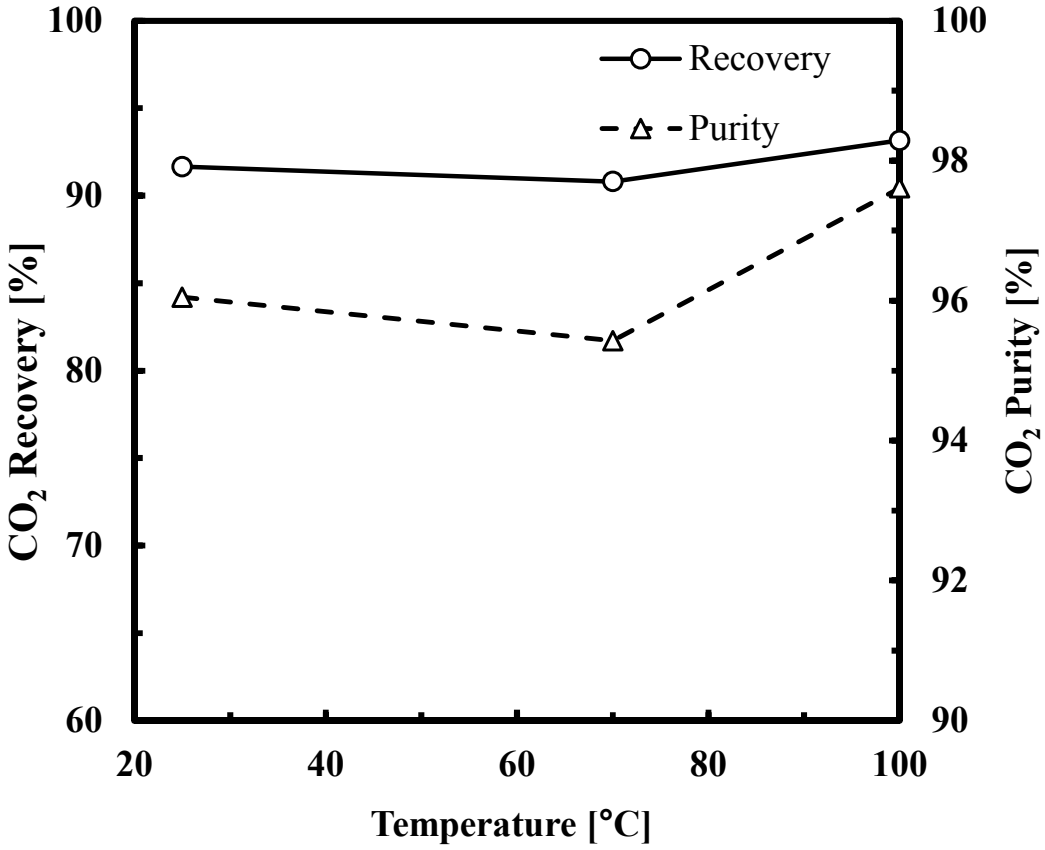


Figure 4.4 Effect of temperature on the $CO_2$ purity and $CO_2$ recovery in the heavy product.

## 4.2 MODEL PREDICTION OF THE PSA EXPERIMENTAL RESULTS

In a previous study, the dynamic adsorption process simulator (DAPS) was validated against the experiments performed in the 1-bed PSA apparatus. The DAPS model was validated against the experimental data obtained in the five runs in single bed PSA apparatus described in previous study. This validated DAPS was used to predict the experimental results of the 4-bed PSA apparatus. The simulations was performed using the equilibrium and kinetic information of the 13X zeolite for the given gases independently in separate measurement methods. As explained before the equilibrium isotherm of both

$CO_2$ and $N_2$ on 13X zeolite was obtained using the micromeritics ASAP 2010 for three different operating temperatures. The mass transfer coefficients of $CO_2$ and $N_2$ was obtained using the rapid pressure swing apparatus (RPSA). In these simulations one parameter mass transfer coefficient with energy balance was used. The main heat transfer resistance is between the solid and gas phase inside of the column wall. In order to remove the heat transfer of the wall and outside the wall thickness was considered negligible. The heat transfer coefficient was obtained by fitting the temperature profile of the bed of a pure $N_2$ purge run. Heat transfer and mass transfer coefficients were not changed in any simulation. Only the valve coefficient of different steps was changed in order to match the pressure history of the bed during a complete cycle.

In Figure 4.5, the model predicted pressure profile of the bed was plotted against the experimental pressure profile of the bed-1 at the periodic state for the entire PSA cycle of run E-1. The PSA cycle consists of 7 steps namely feed step (F), heavy reflux step (HR), pressure equalization down step (E), counter-current blowdown step (CnD), light reflux step (LR), equalization step up (E*) and light product pressurization step (LPP). The experimental data was represented as the open circle whereas the solid line shows the model prediction. As it can be seen from the figure the DAPS can predict exactly the experimental pressure profile of the bed. It is very important to have a correct estimation of the individual component isotherms, mass transfer coefficients and heat transfer coefficients. The pressure profile was matched only adjusting the respective valve coefficients of each step no other parameter was adjusted.

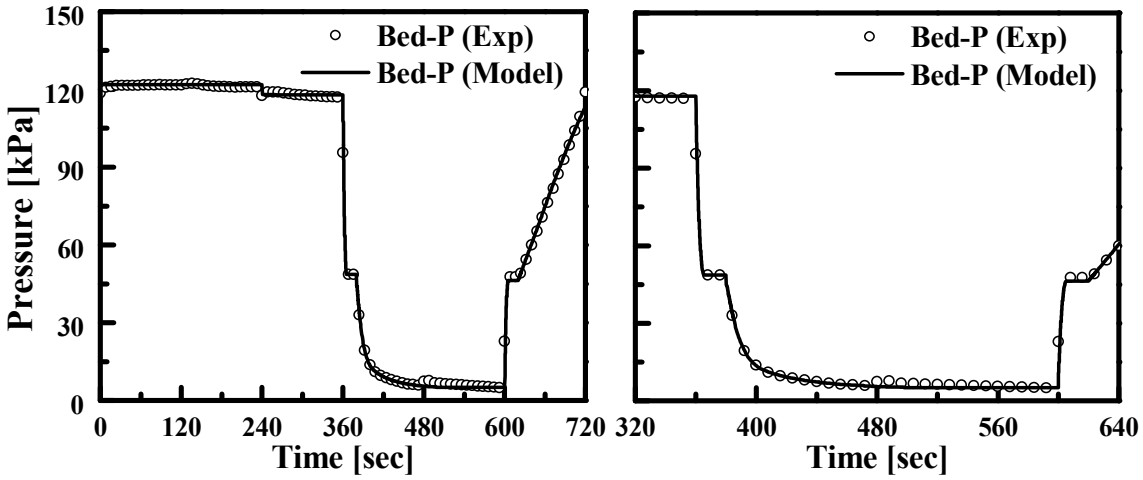


Figure 4.5 Pressure history of Bed-1 during one entire cycle for E1, plotted against the pressure history as predicted by simulation (M-1).

In Figure 4.6, the experimental temperature profiles at periodic state for seven different thermocouples in the bed-1 was plotted against the DAPS predicted temperature profiles for the run E-1. The open circles represent the experimental data whereas the solid lines represent the model predictions. The experimental and model prediction of seven thermocouples (T-1 to T-7) were plotted separately in Figure 4.6(a) – (g) in order for better comparison. In Figure 4.6(h) the model prediction of all the thermocouples (T-1 to T-7) are plotted together. The relative locations of the thermocouples along the bed-1 are T-1: 12.68%, T-2: 24.02%, T-3: 35.73%, T-4: 47.26%, T-5: 58.78%, T-6: 70.31%, and T-7: 81.83%. Because of a higher heat of adsorption of $CO_2$ there is a temperature rise during adsorption and the temperature rise indicates the location of the concentration front in the bed. The first peak in the Figure 4.6(a) – (g) is due to the feed gas. The second peak in Figure 4.6(a) - (d) is due to the heavy reflux gas. The temperature rise during the heavy reflux is more than that happens during feed because $CO_2$ concentration is higher in the

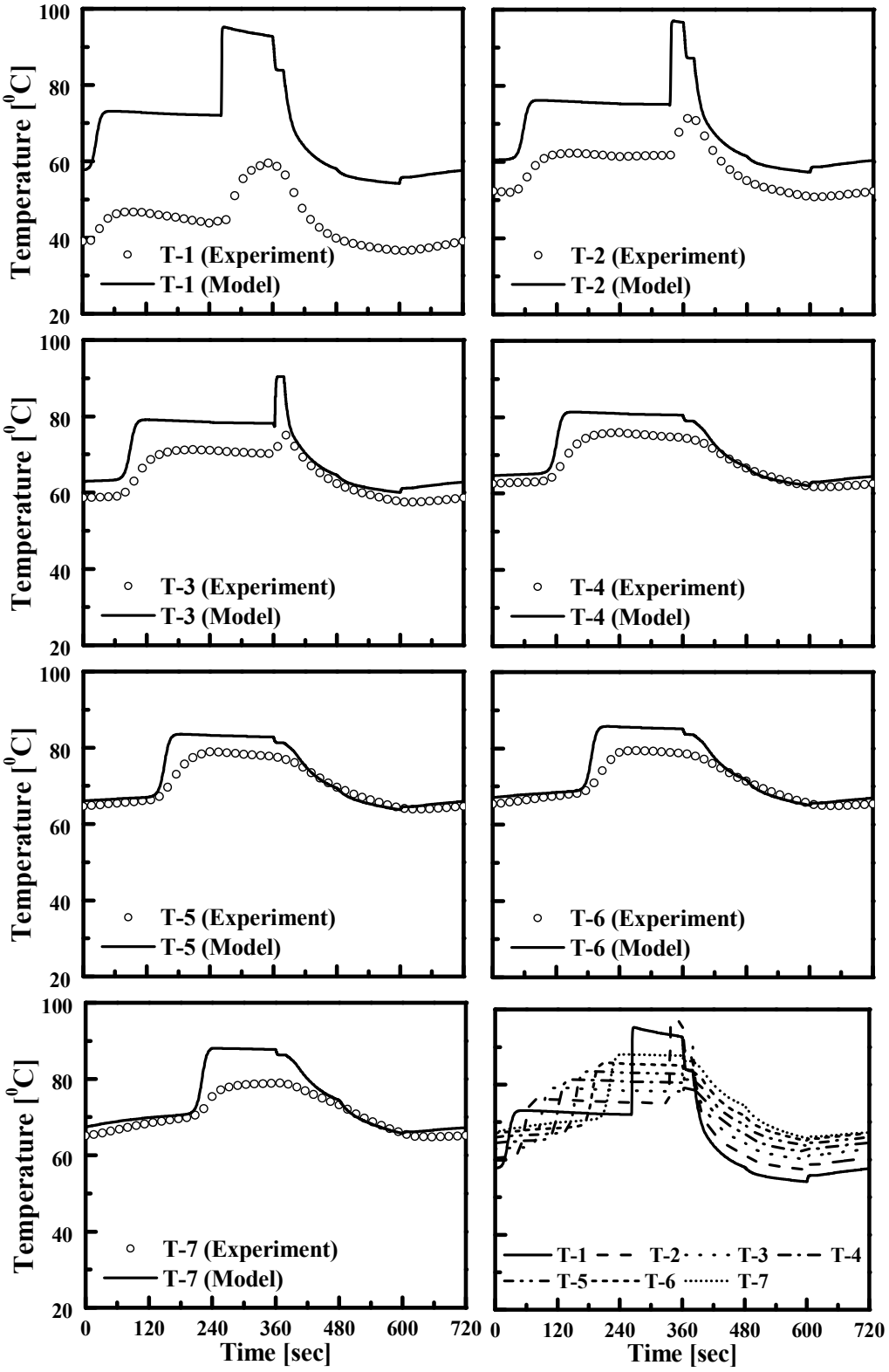


Figure 4.6 Comparison of experiment and model temperature histories for E-1 & M-1. (1:12.68%, 2:24.20%, 3:35.73%, 4:47.26%, 5:58.78%, 6:70.31%, 7:81.83%).

heavy reflux stream. The feed concentration is 15% $CO_2$ whereas the concentration in the heavy reflux stream is in the range 75 - 85% $CO_2$. The progression of the concentration front can be tracked by observing the temperature rise peak in the temperature profile of all the thermocouple. It can be seen that the second peak only reaches until thermocouple T-4 which is 47.26% in the bed that means the front location is between 47.26% and 58.78% of the bed. However, the feed wave front reached until T-7 and a very small amount of $CO_2$ broke through during this experiment. Using the equilibrium isotherms of individual component determined using micromeritics ASAP 2010 and mass transfer coefficients determined from the single gas cyclic experiment in RPSA setup, the model was able to predict accurately the temperature profiles and position of the higher concentration front during the heavy reflux step for the entire PSA cycle for E-1. The comparison of the experiment with simulation prediction of $CO_2$ purity and $CO_2$ recovery in the heavy product for all five runs are shown in Table 4.3. The results show a close agreement between experiments and model.

The energy consumed for each run was calculated using equation (12) and summarized in Table 4.4. The effect on the energy consumed by the PSA process for change in the reflux ratio, CnD pressure and bed temperature were studied. Figure 4.7 shows the energy consumed (kJ/mol of $CO_2$ removed) by the PSA unit cumulatively during the CnD step and the LR step for changing the light reflux ratio ($\gamma$). For each case the energy consumption was calculated for the compressor efficiency 80%. Figure 4.7 shows that the energy consumption increases by increasing $\gamma$. Operating at higher $\gamma$ means more gas exit the LR step, which recycled back completely to the HR step.

| Temp | Exp | Feed $CO_2$ Conc. | $P_L$ | R.R. | HP $CO_2$ Rec [%] | | HP $CO_2$ Pur [%] | |
|---|---|---|---|---|---|---|---|---|
| [°C] | | [%] | [kPa] | [%] | Experiment | Modeling | Experiment | Modeling |
| 70 | E-1 | 16.00 | 5.02 | 2.0 | 91.68 | 88.64 | 96.83 | 95.87 |
| | E-2 | 16.05 | 5.01 | 3.0 | 90.81 | 90.11 | 95.43 | 95.58 |
| | E-3 | 16.05 | 5.12 | 4.0 | 94.06 | 92.10 | 96.54 | 95.60 |
| | E-5 | 16.00 | 6.94 | 4.0 | 87.16 | 86.15 | 95.93 | 95.72 |
| | E-6 | 16.00 | 10.28 | 4.0 | 70.39 | 70.00 | 93.68 | 94.28 |
| | E-11 | 10.04 | 5.06 | 3.0 | 90.62 | 87.32 | 86.79 | 86.24 |
| 100 | E-13 | 16.00 | 5.02 | 3.0 | 93.17 | 91.00 | 97.61 | 96.86 |
| 25 | E-17 | 15.99 | 5.50 | 3.0 | 91.66 | 81.13 | 96.05 | 93.60 |

Table 4.3 Summary of PSA cycle experimental results compared with simulation.

The more energy consumption is due to the higher flow rate. The base case met the DOE criteria of 90% $CO_2$ recovery, 95% $CO_2$ purity and energy consumption of less than 20 kJ/mol $CO_2$ captured.

Figure 4.8 shows the energy consumption for three different CnD pressures (PL), 5, 7 and 10 kPa. The highest pressure of the process (PH) was kept constant for all three runs. As it can be seen from Figure 4.8 that the energy consumption is lower for 7 kPa as

| Experiment | Energy [kJ] | Energy [kJ/mol of $CO_2$] |
|---|---|---|
| E-1 | 5.92 | 17.93 |
| E-2 | 6.26 | 18.63 |
| E-3 | 6.58 | 19.17 |
| E-5 | 5.39 | 16.73 |
| E-6 | 4.42 | 17.10 |
| E-11 | 4.48 | 22.02 |
| E-13 | 6.80 | 20.12 |
| E-17 | 5.03 | 16.70 |

Table 4.4 Energy consumption selected experiments from simulation

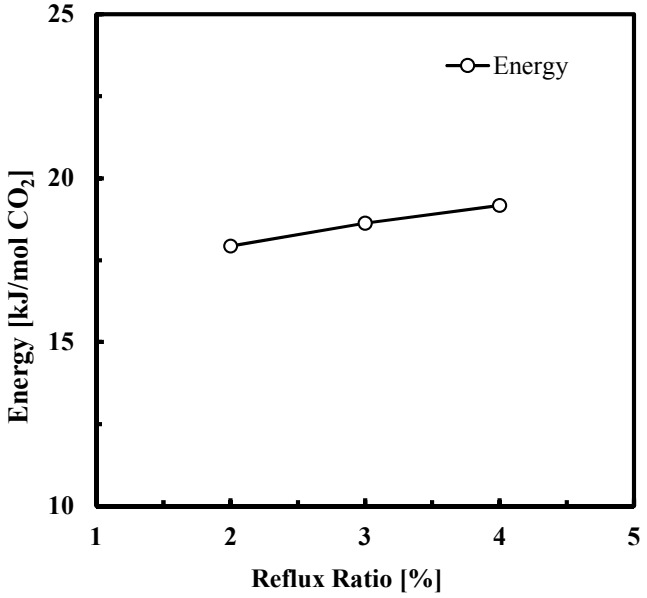


Figure 4.7 Effect of reflux ratio on the energy consumption of the PSA process

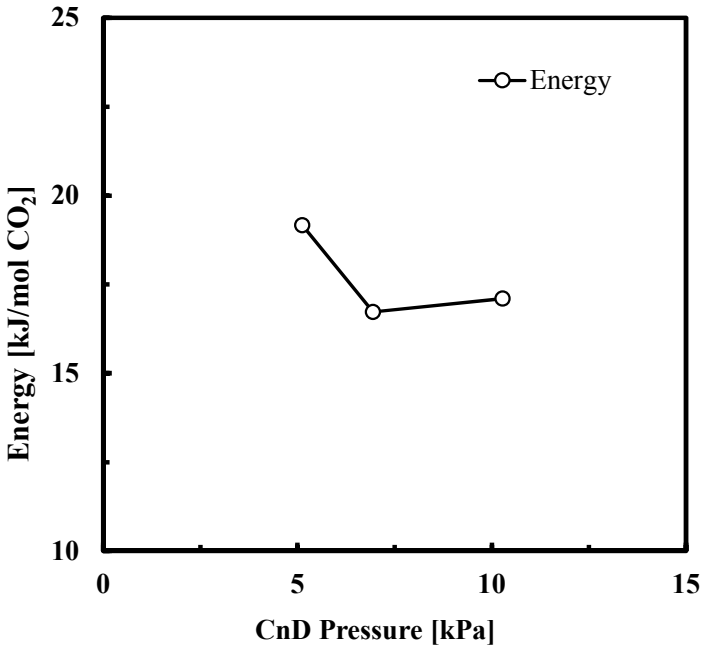


Figure 4.8 Effect of CnD pressure on the energy consumption of the PSA process

compared to 5 kPa as expected. However, the energy consumption increases for 10 kPa compared to that of 7 kPa. For each case, the energy consumption was calculated for compressor efficiency 80%. The higher PL (i.e. lower $\pi$) is not sufficient enough to effectively regenerate the bed during the CnD and LR steps which lowers the $CO_2$ recovery in the HP. Therefore, a higher PL means less work done by the compressor (kJ), the energy consumed (kJ/mol of $CO_2$ produced) is high due to low $CO_2$ recovery in the heavy product.

Figure 4.9 shows the effect of energy consumption (kJ/mol of $CO_2$ captured) for three different temperatures 25, 70 and 100 °C. The energy consumption increases by increasing temperature. From equation (12), it can be seen that the energy consumption is directly proportional to the operating temperature, which explains the increase in energy for increasing temperature.

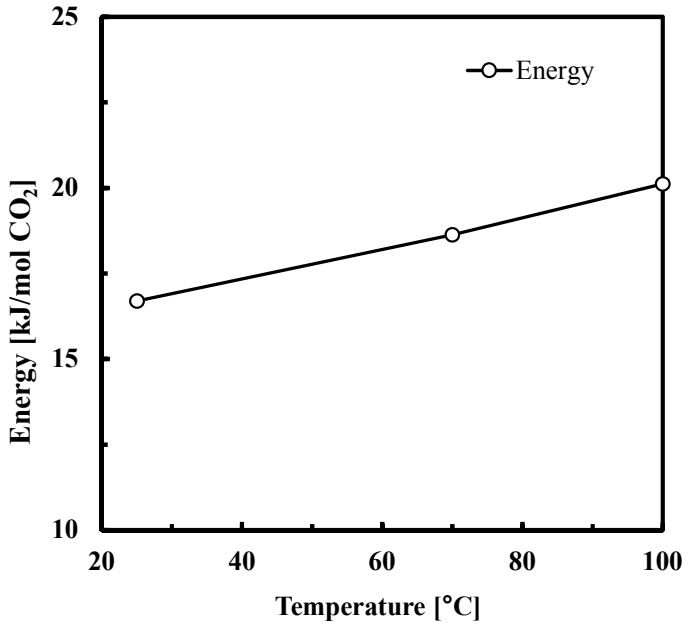


Figure 4.9 Effect of temperature on energy consumption

# CHAPTER 5

# CONCLUSION

A pressure swing adsorption (PSA) process has been described that is cable of separating $CO_2$ from flue gas using 13X zeolite as adsorbent by a dual-reflux PSA cycle. The feed gas considered as a simulated dry flue gas consisting of 15.9% $CO_2$ and balance $N_2$ that was fed at 121 kPa and at 25 °C. A unique combination of cycle steps consisting of three beds was able to produce high purities (>90%) and high recoveries (>90%) of $CO_2$ in the heavy product. The throughput achieved experimentally was 404 $L_{STP}$/hr/kg. A comprehensive experimental study was performed to determine the effect of different process conditions such as feed concentration, purge to reflux ratio, pressure ratio, bed temperature on the $CO_2$ purity, $CO_2$ recovery in the heavy product and the energy consumption (kJ/mol $CO_2$ captured) by the PSA process.

The study showed that purge to feed ratio has significant effect on the process performance. The $CO_2$ recovery increased as the purge to feed ratio was increased. For all the experiment, the total effluent coming out of the LR step was recycled back as the feed to the HR step. By increasing, the purge to feed ratio more $CO_2$ desorbs during the LR step and the bed regenerated better, but it also pushes the high concentration wave front further up the bed during the HR step. A smaller value of the purge to feed ratio causes less regeneration of the bed and the high concentration wave front does not travel through the bed more. Increasing value of the purge to feed ratio also increases the purity and recovery

of the $CO_2$. A higher value of the purge to feed ratio physically means large flow rates exiting from the LR step, which increases the energy consumption of the PSA process.

Pressure ratio also had a significant effect on the $CO_2$ recovery and $CO_2$ purity in the heavy product. Operating at a deeper vacuum resulted in greater $CO_2$ desorption and better bed regeneration. As the CnD pressure ($P_L$) was increased, i.e. pressure ratio decreased the $CO_2$ purity and $CO_2$ recovery both were decreased. The $CO_2$ recovery was decreased when operated at lower pressure ratio causing the energy consumption increase.

The effect of temperature and feed concentration was also studies. The $CO_2$ recovery and $CO_2$ purity in the heavy product increased by increasing the temperature. The energy consumption also increased upon increasing temperature. Three different feed concentration was used 15.9%, 14.59% and 10%. The $CO_2$ recovery and $CO_2$ purity in the heavy product was increased with increasing $CO_2$ concentration in the feed.

A validated DAPS was used to predict a number of experimental results. The DAPS was used to predict the experimental results for different process conditions using equilibrium isotherms of the individual components measured at three different temperatures independently using micromeritics ASAP 2010 and the mass transfer coefficients determined using the single gas cycling using a rapid pressure swing adsorption apparatus. The model successfully predicts the pressure and temperature profiles and performance of each experiment. DAPS successfully capture the location of the concentration front in the bed without any adjustable parameters. The agreement between the experiment and simulation results also validate the single component adsorption isotherm and mass transfer coefficient measure independently. The reason simulation predicted temperature profiles did not match perfectly with the experiment was

that there is only one lumped heat balance was used. This did not account for the difference in temperature between the feed gas and the bed temperature. However, the model does excellent job in predicting the location of the temperature peaks.

# REFERENCES


Agarwal, Anshul, Lorenz Biegler and Stephen E Zitney. "Superstructure-Based Optimal Synthesis of Pressure Swing Adsorption Cycles for Precombustion CO2 Capture." *Industrial & Engineering Chemistry Research* 49 (2010): 5066-5079.

Chaffee, Alan L, et al. "CO2 capture by adsorption: Materials and process development." *International Journal of Greenhouse Gas Control* 1.1 (2001): 11-18.

Chou, Cheng-Tung and Chao-Yuh Chen. "Carbon dioxide recovery by vacuum swing adsorption." *Separation and Purification Technology* 39 (2004): 51-65.

Chue, K T, et al. "Comparison of Activated Carbon and Zeolite 13X for CO2 Recovery from Flue Gas by Pressure Swing Adsorption." *Industrial & Engineering Chemistry Research* 34 (1995): 591-598.

Dantas, Tirzha L.P, et al. "Carbon Dioxide Nitrogen Separation Through Pressure Swing Adsorption." *Chemical Engineering Journal* 172 (2011): 698-704.

Department of Energy. *Energy-Related Carbon Dioxide Emissions*. 2014. < https://www.eia.gov/environment/emissions/carbon/>.

—. *U.S.Energy Information Administration*. 1 April 2016. <https://www.eia.gov/tools/faqs/faq.cfm?id=427&t=3>.

DOE/NETL. "Carbon dioxide capture and storage RD&D roadmap." 2010.

Gomes, Vincent G and Kevin W.K. Yee. "Pressure swing adsorption for carbon dioxide sequestration from exhaust gases." *Separation and Purification Technology* 28 (2002): 161-171.

Grande, Carlos A, Simone Cavenati and Alirio E Rodrigues. *Pressure Swing Adsorption for Carbon Dioxide Sequestration*. Universidade do Porto. Porto, Portugal, 2005.

Haghpanah, Reza, et al. "Cycle synthesis and optimization of a VSA process for postcombustion CO2 capture." *AIChE Journal* 59.12 (2013): 47354748.

Hirose, M, et al. Carbon dioxide separation and recovery system. Japan: Patent 2005262001. 2005.

Internal Energy Agency. "Working party on fossil fuels, CO2 capture at power stations and other major point sources." 2003.

International Energy Agency. "Working party on fossil fuels, solutions for the 21st century: zero emissions technologies for fossil fuels." 2002.

Ishipashi, Michio, et al. "Technology for removing carbon dioxide from power plant flue gas by the physical adsorption method." *Energy Conservation and Management* 37.6-8 (1996): 929-933.

Ito, K, K Otake and M Itoi. Carbon dioxide desorption method. Japan: Patent 2004020393. 2004.

Kikkinides, Eustathios S, Ralph Yang and S Cho. "Concentration and recovery of carbon dioxide from flue gas by pressure swing adsorption." *Industrial & Engineering Chemistry Research* 32 (1993): 2714-2720.

Ko, Daeho, Ranjani Siriwardane and Lorenze T Biegler. "Optimization of Pressure Swing Adsorption and Fractionated Vacuum Pressure Swing Adsorption Processes for CO2 Capture." *Industrial & Engineering Chemistry Research* 44 (2005): 8084-8094.

Krishnamurthy, Shreenath, et al. "CO2 capture from dry flue gas by vacuum swing adsorption: A pilot plant study." *AIChE Journal* 60 (2014): 1830-1842.

Ling, Jianghua, et al. "Effects of feed gas concentration, temperature and process parameters on vacuum swing adsorption performance for CO2 capture." *Chemical Engineering Journal* 265 (2015): 47-57.

Liu, Zhen, et al. "Multi-bed Vacuum Pressure Swing Adsorption for Carbon Dioxide from Flue Gas." *Separation and Purification and Technology* 81 (2011): 307-317.

Lopez, Filipe V.S, Carlos A Grande and Alirio E Rodrigues. "Activated carbon for hydrogen purification by pressure swing adsorption: Multicomponent breakthrough curves and PSA performance." *Chemical Engineering Science* 66 (2011): 303-301.

Marx, Dorian, et al. "CO2 Capture from a Binary CO2/N2 and a Ternary CO2/N2/H2 Mixture by PSA: Experiments and Predictions." *Industrial & Engineering Chemistry Research* 54 (2015): 6035-6045.

Park, Jung-Ho, et al. "Numerical Analysis on the Power Consumption of the PSA Process for Recovering CO2 from Flue Gas." *Industrial Engineering Chemistry Research* 41 (2002): 4122-4131.

Reynolds, Stephen P, Armin D Ebner and James A Ritter. "Carbon dioxide capture from flue gas by pressure swing adsorption at high temperature using K-promoted HTlc: Effects of mass transfer on the process performance." *Environmental Progress* 25 (2006): 334-342.

—. "New Pressure Swing Adsorption Cycles for Carbon Dioxide Sequestration." *Adsorption* 11 (2005): 531-536.

—. "Stripping PSA cycles for CO2 recovery from flue gas at high temperature using hydrotalcite-like adsorbent." *Industrial & Engineering Chemistry Research* 14 (2006): 4278-4294.

Reynolds, Stephen P, et al. "Heavy reflux PSA cycles for CO2 recovery from flue gas: Part I. Performance evaluation." *Adsorption* 14 (2008): 399-413.

Rochelle, Gary T. "Amine scrubbing for CO2 capture." *Science* 325 (2009): 1652-1654.

Sasaki, A, et al. "CO2 recovery in molten carbonate fuel cell system by pressure swing adsorption." *IEEE Transactions on Energy Conversion* 8 (1993): 26-32.

Takmura, Yoshiyuki, et al. "Evaluation of dual-bed pressure swing adsorption for CO2 recovery from boiler exhaust gas." *Separation and Perification Technology* 24 (2001): 519-528.

Webley, Paul A. "Adsorption technology for CO2 separation and capture: A perspective." *Adsorption* 20.2 (2014): 225-231.

Xiao, Penny, et al. "Capture of CO2 from flue gas streams with zeolite 13X by vacuum-pressure swing adsorption." *Adsorption* 14 (2008): 575-582.

Yokoyama, Takahisa. "Japanese R&D on Large-Scale CO2 Capture." *Separations Technology VI: New Perspectives on Very Large-Scale Operations*. Ed. Chris Fell. New South Wales, 2004. <http://dc.engconfintl.org/separations_technology_vi/7>.

Zhang, Jun and Paul A Webley. "Cycle Development and Design for CO2 Capture from Flue Gas by Vacuum Swing Adsorption." *Environmental Science & Technology* 42 (2007): 563-569.

Zhang, Jun, Paul A Webley and Penny Xiao. "Effect of Process Parameters on Power Requirements of Vacuum Swing Adsorption Technology for CO2 Capture From Flue Gas." *Energy Conversion and Management* 49 (2008): 346-356.